Low temperature electrical properties of magnetite and Mn-ferrites

LOW TEMPERATURE ELECTRICAL PROPERTIES OF MAGNETITE AND Mn-FERRITES

Zdeněk Šimša and Victor A.M. Brabers (1)

Institute of Physics, Czechoslovak Academy of Sciences,
180 40 Prague 8, Czechoslovakia
(1)Department of Physics, Eindhoven University of Technology
5600 MB Eindhoven, The Netherlands

Electrical resistivity and thermoelectric power measurements have been made on single crystals of manganese ferrites, $Mn_xFe_{3-4}O_4$ (x = 0, 0.5, 0.7, 0.8, 0.9 and 0.95) in the temperature range 10 K to 300 K. Below the Verwey transition T_v of magnetite, the thermoelectric power is strongly influenced by the oxygen nonstoichiometry of the samples whereas the resistivity exhibits hardly any dependence on the changes of the oxygen content. Starting from the lowest temperatures, the electrical properties are explained in terms of the impurity band, variable range hopping, small polaron band and small polaron hopping conduction mechanisms where the long-range and the short-range orderings have to be taken into account.

Introduction

Extensive experimental and theoretical work have been done to understand the electronic structure and electrical transport mechanisms in magnetite (Fe_3O_4) and other spinel ferrites. Starting with early investigations of Verwey [1,2] who discovered a jump of two-orders of magnitude of the electrical resistivity ρ of magnetite at $T_v \approx 120$ K, a vast number of papers have been devoted to studying of this first-order structural, magnetic and electrical phase transition (see e.g. [2-8]).

In the same time, work on the electrical properties of the "substituted magnetites", i.e. iron-excess mixed ferrites like cobalt ferrites [9], manganese ferrites [10,11], nickel ferrites [12] etc. was going on, revealing that the classical semiconductor one-electron band picture breaks down. A new concept of more or less localized charge carriers (small polarons) was developed to account for the observed electrical, magnetic and optical properties of monoxides, sesquioxides and more complex magnetic oxidic materials (for reviews see e.g. [13-15]). Taking into account a splitting of the conduction levels, it was possible to explain a complex behaviour of the thermoelectric power α near T_v in the case of magnetite [16,17].

However, the observed dependences of electrical properties of ferrites at low temperatures revealed early on that the simple small polaron picture must be modified in at least two ways:

a) impurities present in ferrites introduce band conduction or hopping of charge carriers which becomes important at low temperatures;

b) correlation effects must be introduced into the small polaron theories.

In such a way, the behaviour of the electrical conductivity and thermopower of the fluorine substituted magnetite [18] and the low temperature properties of nickel ferrites [19] were described. Considering the correlation effects of small polarons (leading to short range ordering) Ihle and Lorenz [20] were able to explain the conductivity maximum occurring in magnetite at about 300 K.

In this report, a more detailed investigation of the electrical resistivity and thermoelectric power of several samples of magnetite is made in order to clarify the behaviour of α below T_v. Measurements of electrical properties of iron-rich manganese ferrites give further informations on the influence of substitutional disorder on the behaviour of charge carriers.

Experimental part

Samples.

Single crystals of magnetite and manganese ferrites in the system $Mn_xFe_{3-x}O_4$ were prepared by the travelling - molten - zone technique as described elsewhere [21]. After growth the single crystal rods (approx. 5mm in diameter) were additionally heat-treated at T_h=1470 K for 70 hours and slowly cooled to room temperature in controlled atmospheres, to secure the adjusted oxygen stoichiometry. From the rods, rectangular samples of 1x5x12 mm^3 were cut and finely polished. The remaining parts of the crystals were used for chemical analysis to determine final contents of cations and the active oxygen. Results of the analysis, partial oxygen pressures during heat-treatment and crystal axes are listed in Table 1. It was found that the gradients in chemical compositions along or across the samples were within the error limits of chemical analysis (i.e. 0.02 and 0.002 for x and γ resp.). Electrical contacts were made by rubbing in an eutectic In-Ga alloy at the opposite faces of the samples.

Electrical resistivity.

A four point dc potentiometric method was used to determine the electrical resistivity

Table 1
Final compositions and treatment conditions of $Mn_xFe_{3-x}O_{4+\gamma}$

Sample	x	γ	log pO_2	T_h(K)	axis
A	0	0.046	-6.0	1370	<110>
B	0	0.008	-7.6	1420	<110>
C	0	0.007	-8.3	1420	<110>
D	0	0.006	-8.5	1420	<110>
E	0	0.005	-8.8	1420	<110>
F	0	0.009	-7.6	1400	<110>
G	0	0.004	-10.2	1470	<110>
0.5	0.52	0.009	-6	1470	<100>
0.7	0.70	0.009	-6	1470	<100>
0.8	0.79	0.005	-6	1470	<100>
0.9	0.90	0.002	-6	1470	<111>
0.95	0.95	0.002	-6	1470	<110>

0018-9464/88/0300-1910$01.00©1988 IEEE

of the low resistive samples at various current densities. Resistances (accuracy better than 1%) were determined at such current values where Ohm's law was fulfilled. At low temperatures when resistances reached 10^6 Ω a voltage drop at probes was determined using a Keithley 640 electrometer with the input resistance exceeding 10^{15} Ω. At very high resistances (>10^{11} Ω) a two point method exploiting a feed-back loop of the electrometer was used.

Sample temperature was varied by means of a liquid helium continuous-flow cryostat; temperature control (with accuracy of 0.1 K) was achieved with a DTC 2 (Oxford instruments) controller connected to a C.L.T.S. sensor.

Thermoelectric power.

To determine the thermoelectric power per 1 K (Seebeck coefficient α) the opposite ends of the sample were clamped in the arms of the aluminized sample holder (enabling a good thermal contact and securing a high electrical isolation of sample from the holder). The arms could be individually heated to establish a temperature gradients up to 5 K/cm along the sample in both directions. Temperatures of arms were measured by Au+0.03 %Fe vs.chromel thermocouples and the thermopowers generated by temperature gradients were determined by open input Keithley 640 electrometer. Slopes of the thermopower vs. temperature differences plots were used to calculate the values of α.

Results

Magnetites.

Temperature dependences of the electrical resistivities of magnetite samples in log ρ vs. 1/T representation are shown in Figs. 1,2.

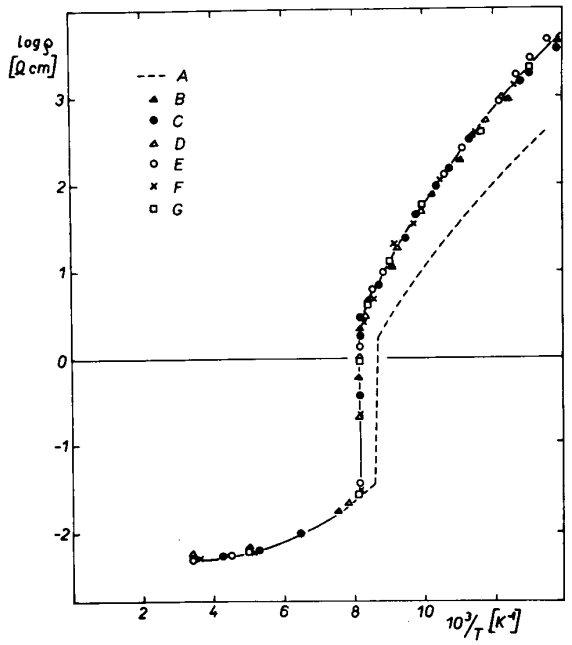

Fig. 1 Temperature dependences of the resistivity of magnetites in the 80 K to 300 K range (see Table 1 for sample details)

It is seen that with the exception of the highly non-stoichiometric sample A all other specimens have identical temperature dependences of resistivity down to 10 K. Although the concept of activation energy has different meanings in various theories of transport mechanisms it is worthwhile (for the sake of comparison and estimation) to define a conductivity activation energy as

$$(1) \qquad \epsilon(eV)=1.895*10^{-4}d(\log\rho)/d(1/T)$$

Values of ε as determined for the magnetite samples just above and just below the Verwey transition and at 10 K are listed in Table 2.

Table 2
Activation energies for magnetites
(see Table 1 for sample details)

Sample	ε(T>Tv)	ε(T<Tv)	ε(T=10 K)
A	0.05	0.12	0.006
B to G	0.05	0.15	0.008

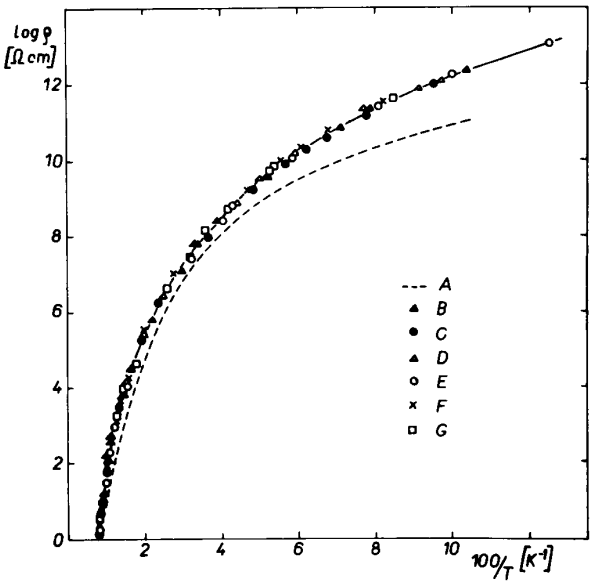

Fig. 2. Temperature dependences of the resistivities of magnetites at 10 K to 100 K (see Table 1 for sample details).

The temperature dependences of the thermoelectric power for representative samples of magnetite are depicted in Fig. 3. The other samples display intermediate behaviour and, to avoid possible confusion, were not included in Fig.3. A salient feature is the strong dependence of α below T_V on the heat treatment conditions of samples, as opposed to the small changes of α above T_V with α remaining practically constant up to room temperature. The most remarkable is the behaviour of sample G where a transition from n-type to p-type conductivity occurs at 100 K followed by a maximum at 80 K and another transition to n-type at about 50 K. Below 40 K all samples behave in a similar manner with α⟶0 for T⟶0.

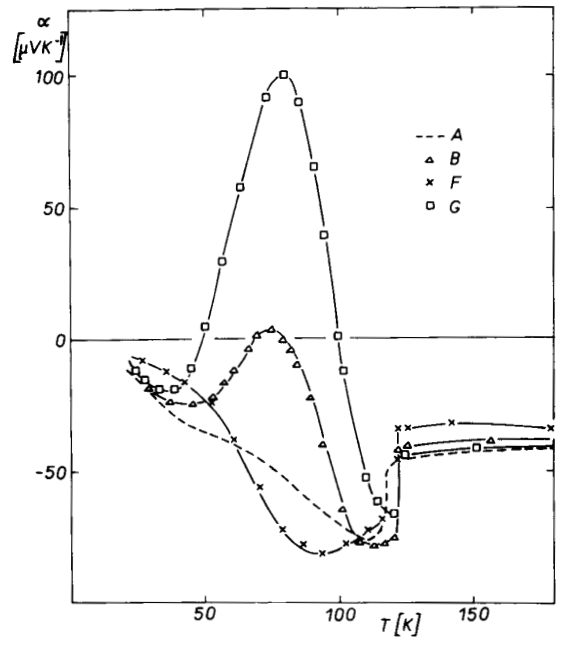

Fig. 3. Temperature dependences of the Seebeck coefficient α for magnetite samples.

Mn ferrites.

Temperature dependences of the electrical resistivities of manganese ferrites are shown in Figs. 4 and 5. At higher temperatures (Fig.4), resistivities increase with rising manganese content while the activation energies ϵ, decrease attaining the minimum value for x= 0.9 - see table 3. Below 100 K (Fig.5) the sequence of resistivities is altered, resulting in a reversed succession of ρ with x. The only exception is x=0.95 sample for which ρ and ϵ are larger than the values of the other samples down to 15 K.

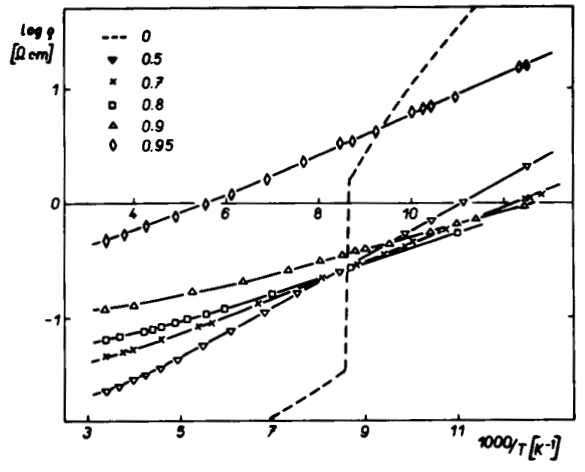

Fig. 4. Temperature dependences of the electrical resistivities of Mn ferrites at 80 K to 300 K range. The symbols indicate the various contents of manganese.

Table 3
Activation energies for Mn-ferrites

Sample	ϵ (T=100 K)	ϵ (T=10 K)
0.5	0.044	0.009
0.7	0.034	0.008
0.8	0.030	0.007
0.9	0.025	0.005
0.95	0.036	0.008

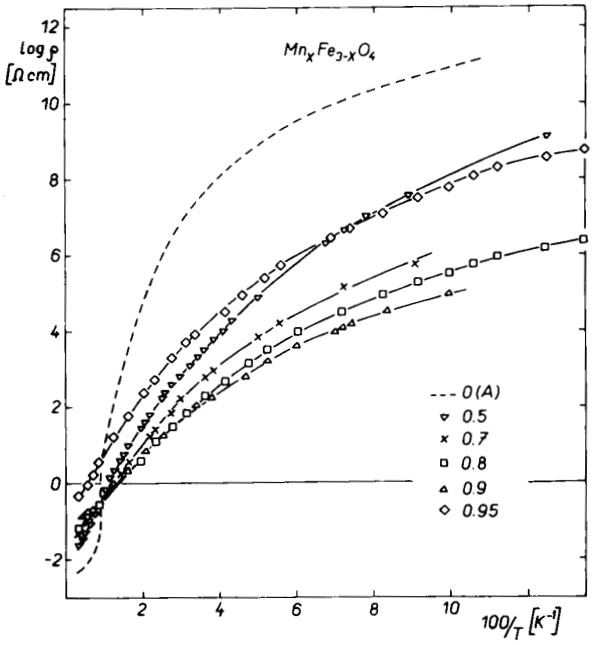

Fig. 5. Temperature dependences of the electrical resistivities of Mn-ferrites in 10 K to 100 K region. The symbols indicate the various contents of manganese.

In Fig. 6 temperature dependences of the Seebeck coefficients of Mn-ferrites are represented. Starting at room temperature a slight increase of α in decreasing temperatures is first observed. In the 150 K to 50 K region α reaches a maximum followed by a regular decrease (down to zero) when T → 0.

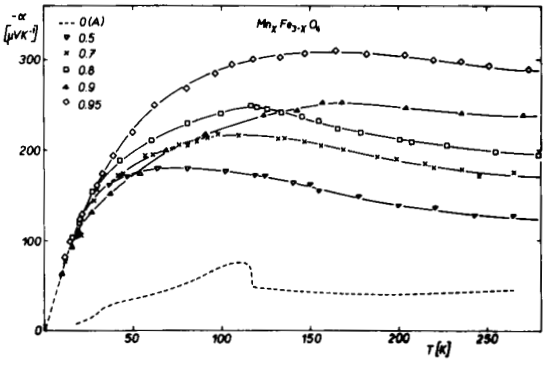

Fig. 6. Temperature dependences of the Seebeck coefficient of Mn-ferrites. The symbols indicate the various contents of manganese.

Discussion

A number of conduction mechanisms were suggested to account for the complex behaviour of the temperature dependence of the electrical resistivity of magnetite. In agreement with other experiments [22,23] our low temperatures measurements confirm the importance of the impurity conduction mechanism. The impurities in the form of cation vacancies are introduced in magnetite as a result of the oxygen nonstoichiometry (see Table 1) acting as donor centres. In manganese ferrites, the impurity levels are also formed by the electrons trapped at octahedral Mn^{3+} ion sites or in the neighbouring iron ions (for discussion of the trapping centers see [10,11]. The theory of correlated hopping transport leading to impurity band conduction [24] yields for the temperature dependence of resistivity the following formula

$$\rho = \rho_0 T^{-n} \qquad (2)$$

Relation (2) seems to be well fulfilled in our measurements as may be seen on Fig. 7 which shows the linear dependence of $\log\rho$ vs. $\log T$ at $T < 40$ K.

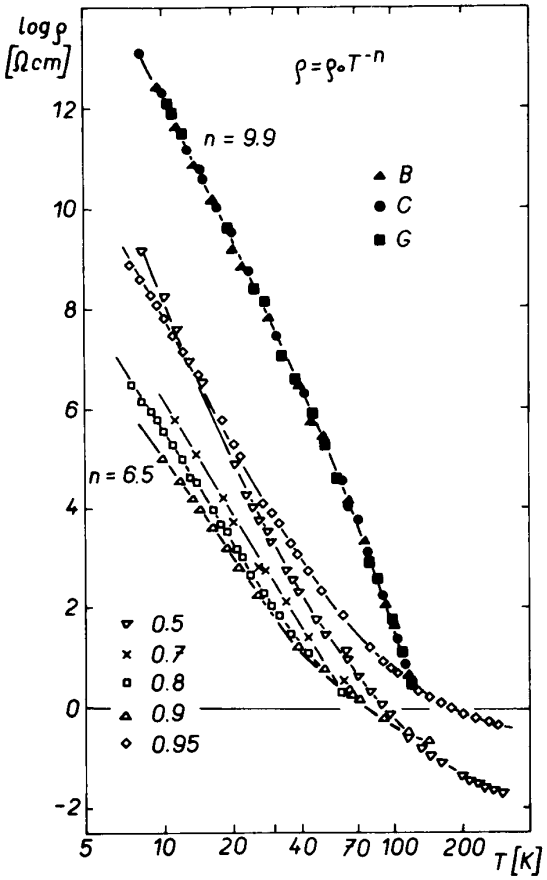

Fig. 7. Demonstration of the $\rho = \rho_0 T^{-n}$ plots for magnetites (full signs) and Mn ferrites (open signs). The symbols indicate the various sample compositions.

Such a relationship has also been found recently in nickel ferrous ferrites [19]. Correlated hopping is also supported by measurements of the thermopower where at low temperatures the relation after [25]

$$\alpha \approx T^{1/2} \qquad (3)$$

seems to be obeyed by magnetite as well as by Mn-ferrite samples.

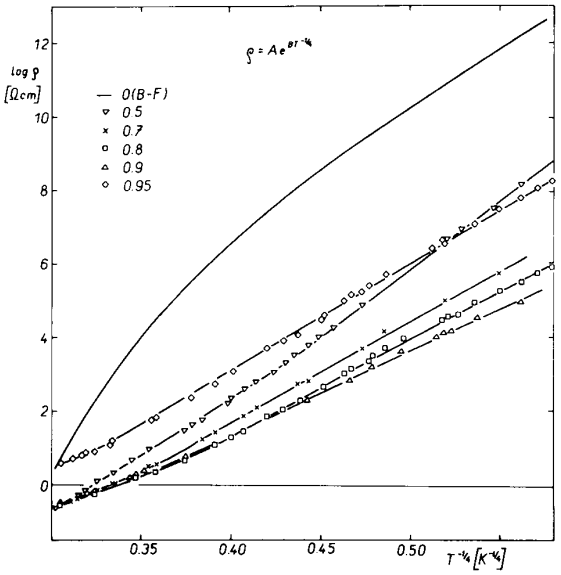

Fig. 8. Demonstration of the Mott's law for magnetites and Mn-ferrites. Symbols indicate the various sample compositions.

At higher temperatures ($T > 40$ K) the variable range hopping yielding the Mott's law

$$\rho = A\exp(B/T^{1/4}) \qquad (4)$$

becomes a more appropriate description in the case of manganese ferrites as shown on Fig. 8. In magnetite, however, relation (4) seems to be satisfactorily obeyed only at low temperatures ($T < 20$ K) and at temperatures just below T_V (cf. also [22]), the intermediate region being the most difficult to interpret. Let us recall the complicated behaviour of α for magnetite samples and the occurence of maxima in Mn-ferrites. The latter are similar to maxima encountered in fluorine-substituted magnetites [18] and nickel ferrites [19] and may be seen as an evidence for the formation of the Coulomb gap in these materials (see discussion e.g. in [5]).

The behaviour of the electrical conductivity of magnetite above T_V has been successfully explained by the simultaneous contribution of small polaron hopping and small polaron band conduction taking into account short-range ordering effects [20]. The behaviour of manganese ferrites above 100 K, may instead be interpreted in the frame of the ordinary nearest neighbour hopping of small polarons as was demonstrated earlier [26].

Conclusions

The conduction mechanism in magnetite and iron-rich manganese ferrites below room temperature has a rather complex character. At low temperatures (T<40 K), a correlated many electron hopping mechanism of localized charge carriers predominate with high resistivities, low activation energies and thermopower varying as $T^{1/2}$. At higher temperatures (40 K < T < 120 K) a variable range hopping mechanism becomes important obeying Mott's law and leading to maxima in the temperature dependences of the thermopower of manganese ferrites. In magnetite, the thermopower in this particular region is very sensitive to the specific dopants, to the degree of ogyxen stoichiometry and to the conditions of heat-treatment. At the Verwey transition of magnetite a jump in electrical properties is caused by the disappearence of the long-range ordering of charge carriers. A certain degree of a short-range ordering above T_v is responsible for the occurence of the conductivity maximum at about 300 K. The electrical properties of Mn-ferrites above 100 K are explained by nearest-neighbour small polaron hopping.

References

[1] E.J.W. Verwey and P.W. Haayman, "Electronic conductivity and transition point of magnetite," Physica, vol. 8, pp. 979-987, 1941.

[2] P.A. Miles, W.B. Westphal and A. von Hippel, "Dielectric spectroscopy of ferromagnetic semiconductors", Rev. Mod. Phys., vol. 29, pp. 279-307, 1957.

[3] B.A. Calhoun, "Magnetic and electric properties of magnetite at low temperatures," Phys. Rev., vol. 94, pp. 1577-1585, 1954.

[4] I.G. Austin and N.F. Mott, "Polarons in crystalline and non-crystalline materials" Adv. Phys., vol. 18, pp. 41-102, 1969.

[5] N.F. Mott, "Hopping conduction and the Coulomb gap," Festkörperprobleme, vol. 19, pp. 331-361, 1979.

[6] N.F. Mott, "Materials with mixed valency that show a Verwey transition," Phil. Mag. vol. B42, pp. 327-335, 1980.

[7] S. Iida, "Structure of Fe_3O_4 at low temperatures," Phil. Mag., vol. B42, pp. 349-376, 1980.

[8] J.M. Honig, "Electrical transitions in metal oxides," J. Sol. St Chem., vol. 45, pp. 1-13, 1982.

[9] G.H. Jonker, "Analysis of the semiconducting properties of cobalt ferrite," J. Phys. Chem Solids, vol. 9, pp. 165-175, 1959.

[10] F.K. Lotgering, "Semiconduction and cation valencies in manganese ferrites," J. Phys. Chem. Solids, vol. 25, pp. 95-103, 1964.

[11] Z. Šimša, "The thermoelectrical properties of manganese ferrites," Czech. J. Phys., vol. B16, pp. 919-928, 1966.

[12] B.A. Griffiths, D. Elwell and R. Parker, "The thermoelectric power of the system $NiFe_2O_4$-Fe_3O_4," Phil. Mag., vol. 22, pp. 163-174, 1970.

[13] A.J. Bosman and H.J. van Daal, "Small-polaron versus band conduction in some transition-metal oxides," Adv. Phys., vol. 19, pp. 1-117, 1970.

[14] M.I. Klinger and A.A. Samokhvalov, "Electron conduction in magnetite and ferrites," Phys. Stat. Sol., vol. (b)79, pp. 9-48, 1977.

[15] S. Krupička, Physik der Ferrite und verwandten magnetischen Oxide. Braunschweig: Vieweg, 1973.

[16] A.J.M. Kuipers and V.A.M. Brabers, "Thermoelectric properties of magnetite at the Verwey transition," Phys. Rev., vol. B14, pp. 1401-1405, 1976.

[17] A.J.M. Kuipers and V.A.M. Brabers, "Electrical transport in magnetite near the Verwey transition," vol. B20, pp. 594-600, 1979.

[18] H. Graener, M. Rosenberg, T.E. Whall and M.R.B. Jones, "The low-temperature resistivity and Seebeck coefficient of fluorine-substituted magnetite," Phil. Mag., vol. B40, pp. 389-399, 1979.

[19] T.E. Whall, K.K. Yeung, Y.G. Proykova and V.A.M. Brabers, "Electrical conductivity and thermoelectric power of nickel ferrous ferrite. Variable range hopping and the Coulomb gap," Phil. Mag., vol. B54, pp. 505-521, 1986.

[20] D. Ihle and B. Lorenz, "Small-polaron conduction and short-rangre order in Fe_3O_4," J. Phys. C: Sol. State Phys., vol. 19, pp. 5239-5251, 1986.

[21] V.A.M. Brabers, "The preparation of tetragonal single crystals in the $Mn_xFe_{3-x}O_4$ system," J. Cryst. Growth, vol. 8, pp. 26-28, 1971.

[22] J.R. Drabble, T.D. Whyte and R.M. Hooper, "Electrical conductivity of magnetite at low temperatures," Solid State Commun., vol. 9, pp. 275-278, 1971.

[23] Z. Šimša, O. Schneeweiss, "Electrical conduction of magnetite and some Mn-ferrites at low temperatures," Czech. J. Phys., vol. B22, pp. 1331-1334, 1972.

[24] M.L. Knotek and M. Pollak, "Correlation effects in hopping conduction: A treatment in terms of multielectron transitions," Phys. Rev., vol. B9, pp. 664-681, 1974.

[25] I.P. Zvyagin, "On the theory of hopping transport in disordered semiconductors," Phys. Stat. Sol., vol. (b)58, pp. 443-449, 1973.

[26] Z. Šimša, J. Šimšová and V.A.M. Brabers, "Electrical conductivity in manganese ferrites," in Proceedings of the ICPS, Warsaw 1972, vol. 2, pp. 1294-1299.

HIGH MAGNETIC FIELD STUDY OF THE NORMAL SPINEL MnV_2O_4

R. Plumier, M. Sougi
Service de Physique du Solide
et de Résonance Magnétique
CEN-Saclay, 91191 Gif-sur-Yvette cedex France

Abstract

Detailed magnetization measurements are performed up to H = 110 kOe in the temperature range 4.2K < T < 70K on the ferrimagnetic normal spinel MnV_2O_4 ($T_c \simeq 56K$). In the (M,T) plane, all isofield curves display hysteresis loops which are located between two temperatures $T_a(H_i)$ and $T'_a(H_i)$ increasing with H_i. From these T_a and T'_a values, we derive a (H,T) phase diagram delimitating five magnetic regions which is in excellent agreement with the set of isotherm magnetization curves. It is observed that the $T_a(H)$ curve intersects the T axis of the (H,T) diagram at $T^* \simeq 53K$ which, in recent neutron diffraction experiments at H = 0, has been shown to be the temperature of a first order transition from a triangular magnetic configuration present in the tetragonal lattice to a Néel configuration in the cubic lattice. It is then assumed that both $T_a(H)$ and $T'_a(H)$ are first order transition lines, the increased stability of the triangular configuration with H being discussed in terms of a large spin-orbit coupling of the V^{3+} magnetic moments.

Introduction

Recent neutron diffraction experiments[1] performed at various temperatures and zero magnetic field have shown that the normal ferrimagnetic spinel, MnV_2O_4, is tetragonal up to $T^* \simeq 53K$ and is cubic at all $T > T^*$. Up to T^*, the magnetic structure is found to be a triangular one with a canting of the V^{3+} magnetic moments on the octahedral sites (Fig. 1.a). On the other hand, in the temperature range $T^* < T < T_c$ ($T_c \simeq 56K$ [2]), the magnetic structure displays the simple antiparallel or Néel configuration (Fig. 1.b). We also observed[1] that up to $T = T^*$, within experimental limits, the nuclear cell parameters keep the same values a = 8.517Å, c = 8.448Å, the transition to a cubic cell at T^* taking place without sizable volume change (a_c = 8.495Å). At $T = T^*$, we also observed that, together with a sudden modification of the magnetic structure which changes from the triangular to the Néel configuration (Fig. 1), a reduction of lengths by about 20% of the magnetic moments lengths is taking place for both the Mn^{2+} and V^{3+} ions respectively located on the tetrahedral (or A) and on the octahedral (or B) sites of the spinel structure. The transition at $T = T^*$ was then assumed[1] to be a first order one, a character confirmed by preliminary magnetization measurements which revealed the existence of a magnetic hysteresis in the temperature range $T^* < T < 58K$.

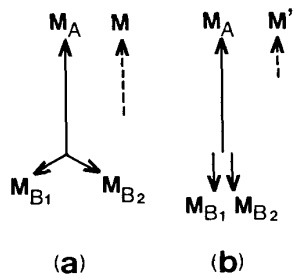

Fig. 1 : Magnetic structures in MnV_2O_4 (a) triangular configuration (b) Néel configuration.

Experimental part

Detailed magnetization measurements have just been performed in our laboratory up to H = 110 kOe and at various temperatures in the range 4.2K < T < 70K on the same powdered specimen of MnV_2O_4 used in the neutron diffraction experiments[1]. Starting at 4.2K, the magnetization curves are obtained by 5K steps, whereas in the temperature range 50K < T < 65K, the experiments are performed by 0.5K steps. Between every experiment, the sample is heated up to T = 70K and then slowly cooled down to the temperature of the experiment. In order to detect possible remanence effects, the magnetization curves are first obtained by increasing the magnetic field H and then by decreasing H (Fig. 2). In

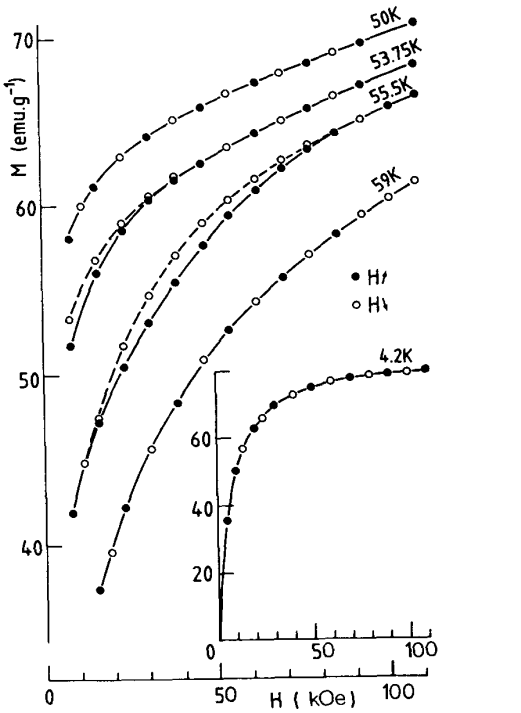

Fig. 2 : Part of the magnetization curves obtained at various temperatures up to H = 110 kOe on both sides of T^* and T_c. The magnetization curve obtained at T = 4.2K may be found in the insert.

0018-9464/88/0300-1915$01.00©1988 IEEE

all cases, the temperature resolution is better than 0.05K and the relative errors in the magnetization never exceed 2×10^{-4}. We have also performed isofield measurements at eleven fixed H values in the range 1 to 110 kOe (Fig. 3). In this kind of experiments, the sample being first heated up to T = 70K is then slowly cooled down to T = 50K. Definite magnetic fields H_i are then applied and the magnetization intensities are determined by increasing the temperature up to T = 65K by 0.25K steps. Keeping the same fixed H_i, the sample is then cooled down to T = 50K by 0.25K steps, the magnetization being determined again at all temperatures. It may be observed (Fig. 3) that in the (M,T) plane, hysteresis loops are obtained at all H_i in this type of experiments. Whereas the width of such loops keeps the almost fixed value $\Delta T \simeq 2K$ whatever H_i, we notice (Fig. 3) a slight decrease of the loop surfaces at increasing H_i. It is seen in Fig. 3 that, up to H_i = 110 kOe, both $T_a(H_i)$ and $T_a'(H_i)$ values which correspond respectively to the smaller and higher temperatures between which the hysteresis is observed are increasing with increasing H_i.

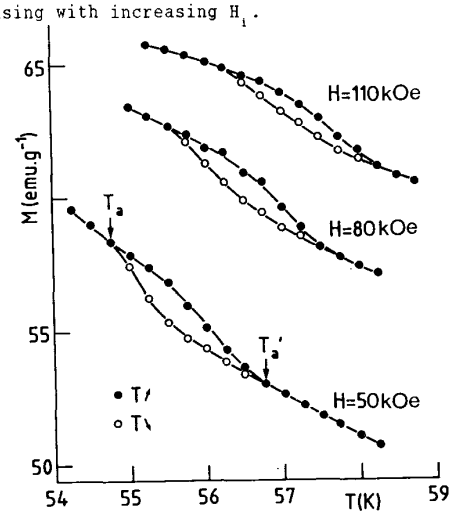

Fig. 3 : Isofield curves obtained at various magnetic fields showing the existence of hysteresis loops between $T_a(H_i)$ and $T_a'(H_i)$ values increasing with H_i.

Phase diagram

From the experimental $T_a(H_i)$ and $T_a'(H_i)$, the (H,T) diagram depicted on Fig. 4 may then be obtained. We find that the extrapolated $T_a(H)$ curve intersects the T axis of that diagram (Fig. 4) very near the value $T = T^*$ at which our previous neutron diffraction experiments[1] performed at H = 0 have shown the existence of a first order transition for both the nuclear and magnetic structures. It may then be assumed that the $T_a(H)$ curve on Fig. 4 is a first order line along which the transition from a tetragonal to a cubic cell starts taking place at finite H_i whereas the $T_a'(H)$ curve corresponds to the temperature at which such a transition is fully achieved for all crystallites. Our experiments also confirm that T_c ($T_c \simeq 56K$ [2]) is an isolated second order transition point in the (H,T) diagram as it is in the case of a simple ferromagnet. From the foregoing it may then be inferred that, in addition to the paramagnetic P phase and the triangular and Néel ordered magnetic configurations, the (H,T) plane (Fig. 4) contains two further regions called I and II located between the curves $T_a(H)$ and $T_a'(H)$.

Region I contains a mixture of triangular and Néel configurations whereas a mixture of triangular configuration and paramagnetic phase P exists in region II. This (H,T) phase diagram suggests that, in the case of magnetization curves determined up to H = 110 kOe at definite temperatures, hysteresis effects should only be expected in the temperature range $T^* < T < 58K$. This is nicely confirmed by the set of magnetization curves depicted in Fig. 2. In the case of such experiments performed at $T_f < T < 58K$ where T_f ($T_f \simeq 54.75K$) is the extrapolated value of the $T_a'(H)$ curve on the T axis (Fig. 4), a closed hysteresis loop in the (M,H) plane is expected. Such a loop is indeed observed in the case of the experiment performed at T = 55.5K (Fig. 2). On the other hand, in the temperature range $T^* < T < T_f$, an open loop is expected as it is indeed observed in the case of the experiment performed at T = 53.75K (Fig. 2).

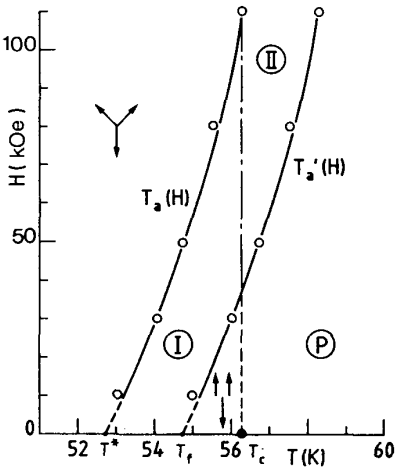

Fig. 4 : (H,T) phase diagram obtained from the set of isofield curves. The triangular and Néel magnetic configurations are depicted in addition to the paramagnetic phase P and to the phases I and II explained in the text.

Discussion

As was mentioned in Ref.[1], the first order transition observed in MnV_2O_4 at T^* and H = 0 is quite exceptional as it takes place at a temperature about 5% lower than T_c between a triangular magnetic configuration superposed on a tetragonal lattice and a Néel configuration lying on a cubic lattice. The results we are reporting here reveal that, up to the highest laboratory field of 110 kOe, an important increase of the first order transition temperature T_a as a function of H is taking place with $\Delta T_a/\Delta H \simeq 0.032K \times kOe^{-1}$. Let us note that the situation existing in MnV_2O_4 is distinct from most first order transitions reported in the past in magnetic compounds and which take place between an ordered magnetic structure and the paramagnetic phase. Such a behaviour is usually explained by large magnetostriction effects as it is, for instance, in the case of the extensively studied MnAs[3]. Although the behaviour observed in region II (Fig. 4) is somehow reminiscent of the observations performed near T_c on MnAs[3], such an explanation based on magnetostriction

is by no means satisfactory in the case of MnV_2O_4. In particular, it is recalled that the transition at T^* takes place without sizable volume change [1], a situation ruling out a possible lowering of the total free energy tied to a strong dependence of the magnetic exchange constants on distance. On the other hand, the observed[1] reduced value $M = 1.34\mu_B$ at $T = 2K$ for the $S = 1$ ion V^{3+} points out the important part played by the spin-orbit coupling in the case of this $3d^2$ ion located in the trigonally distorted octahedral B site of the spinel structure. The importance of this coupling is also revealed by the large anisotropy field of about 150 kOe[2] which manisfests itself by the rounded shape of the magnetization curves (Fig. 2). As these curves are similar on both sides of T^* and T_c, it may then be concluded that cooperative spin-orbit coupling, leading to an overall tetragonal distortion of the spinel lattice, exists for all crystallites only at $T < T_a$ (H). Let us finally point out, as has already been suggested in Ref.[2], the inapplicability of the Yafet-Kittel theory [4] for the stability in the spinel structure of a triangular configuration when large spin-orbit coupling has to be considered in addition to the Heisenberg antiferromagnetic interactions between A-B and B-B first nearest neighbours.

References

[1] R. Plumier and M. Sougi, Solid State Comm. 64, 53, (1987)
[2] K. Dwight, N. Menyuk, D. Rogers and A. Wold : Proc. Int. Conf. Magnetism, Nottingham 1964, 542.
[3] R.W. de Blois, D.S. Rodbell, Phys. Rev. 30, 1347 (1963).
[4] Y. Yafet, C. Kittel, Phys. Rev. 87, 290 (1952).